

Probabilistic data-driven turbulence closure modeling by assimilating statistics

Sagy R. Ephrati*¹

¹Department of Mathematical Sciences, Chalmers University of Technology and University of Gothenburg, 412 96 Gothenburg, Sweden

Abstract

A framework for deriving probabilistic data-driven closure models is proposed for coarse-grained numerical simulations of turbulence in statistically stationary state. The approach unites the *ideal large-eddy simulation* model [47] and data assimilation methods. The method requires a *posteriori* measured data to define stochastic flow perturbations, which are combined with a Bayesian statistical correction enforcing user-specified statistics extracted from high-fidelity flow snapshots. Thus, it enables computationally cheap ensemble simulations by combining knowledge of the local integration error and knowledge of desired flow statistics. A model example is given for two-dimensional Rayleigh-Bénard convection at Rayleigh number $Ra = 10^{10}$, incorporating stochastic perturbations and an ensemble Kalman filtering step in a non-intrusive way. Physical flow dynamics are obtained, whilst kinetic energy spectra and heat flux are accurately reproduced in long-time ensemble forecasts on coarse grids. The model is shown to produce accurate results with as few as 20 high-fidelity flow snapshots as input data.

1 Introduction

The highly turbulent nature of fluid flows provide a major challenge in the prediction of fluid-dynamical processes. Examples include oceanic and atmospheric flows, relevant to geophysics and climate science, or engineering and industrial applications involving thermal processes. The nonlinearity in the governing equations causes interaction between flow features of different scales, leading to energy distribution over a wide range of scales of motion [57]. Accurate direct numerical simulations (DNS) of fluid-dynamical models thus require very fine computational grids to fully resolve all flow features, and quickly become prohibitively expensive to carry out. Feasible simulation strategies for such systems therefore necessitate a reduction in computational complexity to approximate the flow evolution. Well-established approaches dealing with complexity reduction include reduced-order modeling [67], where the governing equations or associated operators are formulated in a low-dimensional manner, and large-eddy simulation (LES) [63, 37], where the governing equations are spatially filtered and small-scale effects are modelled. The current work focuses on the LES approach.

The spatially filtered equations of motion form the starting point for large-scale LES models. The underlying rationale is that computationally feasible methods can be developed by only capturing the largest scales of motion, since these are most important for the overall flow evolution. The level of detail in the LES solution is determined by the filter width. Explicit LES follows from applying the adopted spatial filter to the governing equations directly. Alternatively, the equations can be filtered implicitly by discretizing differential operators on coarse computational grids. Regardless of the chosen approach, filtering introduces errors and uncertainty in the flow evolution. The filter generally does not commute with the nonlinear terms in the governing equations, yielding a so-called commutation error. In addition, discretization error is introduced on coarse computational grids due to poorly resolved spatial derivatives. One can add modeling terms to the governing equations with the aim of compensating for the errors introduced by filtering and coarsening [39, 56, 62]. We will refer to this as the LES model, although it is also often referred to as the closure model or the sub-filter or sub-grid

*(sagy@chalmers.se)

scale model. Furthermore, filtering introduces uncertainty since it discards information of small spatial scales. Infinitely many fully resolved flow fields will correspond to the same filtered LES field, which makes it impossible to know the exact evolution of the LES solution. Consequently, it is desirable to develop error-correcting LES models that simultaneously quantify the uncertainty in the LES solution.

In this paper, we propose a two-step probabilistic data-driven LES closure modeling strategy with the aim of correcting for undesired coarsening effects on the dynamics whilst modeling the inherent uncertainty. The approach is inspired by the abstract *ideal LES model* [47]. The first step consists of a stochastic perturbation of the flow evolution, based on *a posteriori* collected data from a computationally cheap low-fidelity solver that resolves only the large flow features. The second step is a statistical correction, using data assimilation techniques applied to selected key statistics (or quantities of interests, QoIs) of the high-fidelity data. Thus, we combine knowledge of the local errors of the low-fidelity solver with knowledge of long-time statistics of the high-fidelity reference result. After the data has been collected, the model permits indefinite computationally efficient ensemble simulations of the dynamical system. The method is demonstrated for two-dimensional Rayleigh-Bénard convection, where we focus on kinetic energy spectra and heat flux as key statistics. We will now further elaborate on these model components.

The abstract ideal LES model was derived by Langford and Moser [47] and can serve as a guideline for model development. The model is ideal in the sense that it reproduces single-time, multi-point statistics of the unfiltered solution and minimizes the instantaneous dynamics. It states that the ideal evolution of an LES solution is the average evolution conditional to an infinite number of fully resolved (unfiltered) fields corresponding to the current large-scale (filtered) field. One can probe this distribution of fields using a stochastic forecast ensemble and subsequently approximate the conditional average. Naturally, the model depends on the governing equations, the adopted filter and, in simulations, on the chosen spatial and temporal discretizations. This makes it challenging to approximate the conditional average well. However, empirical approximations can still be found through the use of data.

The field of data-driven LES has seen rapid development in recent years due to the increasing availability of computational resources and accessibility of high-fidelity data. Machine learning is used regularly to train neural networks as LES models [64, 10]. One can distinguish between *a priori* and *a posteriori* learning, which differ in their objective function. *A priori* methods rely only on the high-fidelity data to learn a closure model, for example by minimizing a function of the unfiltered and the filtered solution. This approach can yield accurate short-time predictions, but might also suffer from errors and instabilities due to model-data inconsistency [20, 2]. *A posteriori* methods can overcome this inconsistency, by directly comparing the results of the low-fidelity solver and the high-fidelity data [34]. Consequently, the model will depend on the configuration of the low-fidelity solver. The presently proposed model uses an *a posteriori* approach based on the ideal LES formalism to calibrate a stochastic subgrid-scale model.

Stochasticity is commonly used in geophysical fluid dynamics to model uncertainty [43, 13] stemming from imperfect initial conditions and incomplete models [54]. A prevalent interpretation of stochastic forcing is that it models the chaotic behavior of unresolved small scales on the resolved dynamics. For example, data-informed stochastic models have been developed for the two-scale Lorenz '96 system [51]. This system serves as a low-dimensional model of the atmosphere with variables evolving over different time scales. By replacing the influence of fast variables on the slow variables with data-driven stochastic processes, [6] were able to account for model error. The addition of time-correlated noise further improved the forecasting skill. Other approaches based on data-driven Markov chains [19] have led to state-dependent stochastic processes modeling the effects of unresolved variables yielding a good reproduction of statistics of the resolved variables, such as probability density functions and temporal autocorrelation.

The current method fits in the recent modeling trend in observational sciences where high resolution simulations are replaced by stochastically forced simulations on coarse grids. New types of data-driven stochastic models have been developed for fluid-dynamical systems for the purpose of modeling uncertainty in observations and correct for undesired coarsening effects. For example, the effect of transport noise [45, 53] in advection-dominated geophysical flows has been studied in the context of uncertainty quantification [17, 60, 26] and data assimilation [16]. These studies showed good quantification of uncertainty in advective processes at severely reduced computational costs. Another advantage of stochastic forcing is that it allows simulating outside of the dataset from which the model is calibrated.

The chaotic evolution of turbulent flows prompts the development of stochastic models that reproduce flow statistics rather than pointwise agreement with some reference. Inspired by the nonlocality of turbulence, a space- and time-dependent model can be decomposed via global basis functions for which only the time series are modeled [32, 33], possibly based on statistical data. Examples include the use of include proper orthogonal functions (POD) [11] and Fourier modes to reproduce their respective spectra in coarse numerical simulations of Rayleigh-Bénard convection [28, 24]. [31] employed spherical harmonic functions to develop a stochastic subgrid-scale term with memory effects for barotropic flow, and found good agreement in the resulting energy spectra. Capturing flow statistics instead of the full flow also reduces the amount of data required to calibrate the model. Low-dimensional models with basis functions tailored to user-specified statistics can be derived [21] and used to develop stochastic models at severely reduced computational costs while accurately reproducing selected statistics, as was recently shown for the two-dimensional Navier-Stokes equations [44].

Data assimilation (DA) deals with efficiently incorporating data in predictions and is widely employed in geophysical sciences. DA combines predictions of dynamical systems with observations optimally, taking into account the uncertainty in both these aspects [48, 59]. In the context of DA, filtering¹ of turbulent systems has also been carried out by representing interactions of resolved and unresolved scales as stochastic processes [52]. Recent work has provided a theoretical framework for filtering of dynamical systems by observing statistics only [8], with correcting model errors as a possible application. The observations are often dealt with sequentially in DA, resulting in ‘on-the-fly’ updates of predictions or parameters as new information becomes available. This contrasts with data-driven LES, where model parameters are commonly determined before performing a numerical simulation. Nonetheless, we will show here that DA techniques can be adapted to yield turbulence closure models for coarsened discretized systems.

Coarsening a discretized system will lead to a change in the predicted dynamics. Such a change is not necessarily a cause for concern at sufficiently high resolution. However, severe coarsening induces strong errors and yields numerical solutions converging to a different statistically steady state, as may be observed when measuring statistics of the dynamical system at large lead times. These structural errors can be alleviated by steering predictions towards observations (or specific regions of the state space), thereby increasing their likelihood. This is referred to as *nudging* [4]. A similar concept of continuous data assimilation (CDA) based on interpolated approximations of measurements has been developed for fluid flows [7]. CDA assimilates observations while the predictions are integrated in time via a term that nudges the prediction towards the observation. Theoretical convergence for down-scaled solutions has been proved for the two-dimensional Navier-Stokes equations [14], accompanied by numerical results for this system [36] and two-dimensional Rayleigh-Bénard convection [5, 41]. The CDA approach is similar to the continuous-time 3D-Var DA scheme [18, 12]. Recently, a heuristic data-driven stochastic closure model was derived from the 3D-Var scheme, with the aim of reproducing reference energy spectra. This has been demonstrated for the two-dimensional Euler equations [27], Rayleigh-Bénard convection [24], and quasi-geostrophic flow on the sphere [23]. However, unrealistic dynamics may arise when nudging the solution too strongly [59] and we therefore endeavour to replace ad-hoc modeling assumptions by a structured method based on DA techniques. This leads to a modeling framework from which we derive a nudging approach for turbulent flows. One of the results in this paper is that the proposed model yields realistic instantaneous dynamics while reproducing selected flow statistics in long-time simulations, even when only a small amount of data is available.

The paper is structured as follows. In Section 2, we recapitulate the ideal LES model and its connection to data assimilation, and introduce the two-step probabilistic closure. The closure model and adopted implementation is described for Rayleigh-Bénard convection in 3, after which we assess short-time and long-time results in the cases of plenty training data and sparse training data in Section 4. The paper is concluded in Section 5.

¹The term *filtering* is used both the fields of LES and data assimilation but carries a different meaning in each of the fields. In LES, filtering refers to spatial filtering: a method to determine the level of physical detail to keep in the LES solution. In data assimilation, filtering deals with the sequential updating of a probability distribution function of a random variable as new measurements become available.

2 Two-step probabilistic closure modeling framework

In this section we motivate the use of a two-step closure model based on the prediction-analysis approach used in data assimilation [48]. We first summarize the ideal LES model and describe how it suggests using probabilistic methods with specific data. This relates to the first step of the model. Subsequently, we recall some basic notions from data assimilation and establish a statistical correction as the second step of the closure model.

LES generally starts from a filtered description of the governing equations of motion. The abstract ideal LES model [47] was derived to compensate for unwanted effects caused by underresolving the turbulent flow. It is ideal in the sense that it minimizes the instantaneous error in the evolution of the large-scale dynamics. We follow the notation of [47] and denote by u an unfiltered turbulent field. We let w be a resolvable large-scale field, referred to as an LES field. The filtered variables are denoted by a tilde $\tilde{\cdot}$ and note that w does not necessarily equal \tilde{u} . We consider a field of interest u with an evolution given by $L(u)$, which contains a nonlinear advection term. The filtered evolution reads

$$\frac{\partial \tilde{u}}{\partial t} = \widetilde{L(u)}, \quad (1)$$

which can be expressed as the evolution of the filtered field \tilde{u} as

$$\frac{\partial \tilde{u}}{\partial t} = L(\tilde{u}) + M. \quad (2)$$

In the last equation, M is a model term that appears due to the filtering of the nonlinear advection term, which causes a commutation error. Evaluating M requires (unavailable) explicit knowledge of the unfiltered field and will instead be replaced by a model.

The ideal model is shown to minimize error in the instantaneous evolution of large scales and produce accurate spatial statistics [47]. The fundamental insight in the model derivation is that a spatial filter must discard information to be useful. In other words, it cannot be invertible and maps from a high-dimensional (possibly infinite-dimensional) space of turbulent fields to a lower-dimensional space of LES fields. By additionally imposing that any spatial statistic of the true solution is reproduced by the LES solution, it is shown that the LES field w must satisfy

$$\frac{dw}{dt} = \left\langle \frac{d\tilde{u}}{dt} \middle| \tilde{u} = w \right\rangle. \quad (3)$$

This generalizes the results of [1], who showed that modeling turbulence reduces to approximating conditional averages of statistics.

The evolution of the LES field is rewritten as

$$\frac{\partial w}{\partial t} = L_{\text{LES}}(w) + m(w), \quad (4)$$

where L_{LES} is an approximation of the right-hand side of the original evolution equations, for example obtained as a coarse numerical discretization. Throughout this paper, L_{LES} will be integrated with the low-fidelity solver. The LES model $m(w)$ is an approximation to the ideal subgrid model via

$$m(w) = \langle M(u) | \tilde{u} = w \rangle, \quad (5)$$

$$M(u) = \frac{\partial \tilde{u}}{\partial t} - L_{\text{LES}}(\tilde{u}). \quad (6)$$

The above result holds for general flow configurations, numerical methods, and filters. Nonetheless, it is evident that all these choices will influence the model in practical situations. The flow domain and physical parameters naturally determine the operator L . The chosen filter and numerical discretization, which in itself implicitly induces a filter, influence L_{LES} and thus also affect the ideal subgrid model. However, equations (5-6) indicate how to construct the ideal model once knowledge of the full system is available. In particular, it suggests that measurements of the subgrid force (6) are suited to serve as model input. A simple *a posteriori* approach is adopted here to measure (6), which is further detailed in Section 3.2. Integrating the low-fidelity solver in time when measuring $M(u)$ ensures that effects of

spatial and temporal discretization are included in the measurements. Consequently, the closure model will depend on the adopted numerical method and resolution, which is a desired and necessary feature of the closure model and is furthermore required for consistency when adopting higher resolutions in the low-fidelity solver. The adverse effects of discretization diminish at higher resolutions, resulting in measurements of smaller magnitude and ultimately a diminished closure term.

The presence of the conditional average in the ideal model term motivates using probabilistic simulation strategies in coarse numerical simulations. The average in (5) must be taken over an ensemble of predictions whose probability density function (pdf) matches that of the true LES solution [47]. The conditional average can be estimated with sufficient measurements of $M(u)$ using nonlinear mean square estimation [22]. However, it becomes increasingly difficult to obtain sufficient samples of the state space when its dimension increases [59], making it infeasible to compute good approximations of the conditional average even at a modest resolution of the low-fidelity solver. Theoretically, one can sample from a specific distribution of solutions to approximate the ideal LES evolution. We will refer to this distribution as the ideal distribution. We denote by w_n, w_{n+1} the LES solution at time instances n and $n + 1$ and we assume that the filtered high-fidelity solution \tilde{u}_n is known. If we denote the pdf associated with a random variable by $\mathbb{P}(\cdot)$, then the ideal distribution is expressed as $\mathbb{P}(\tilde{u}_{n+1}|\tilde{u}_n)$. This distribution can be approximated from a given filtered initial condition by taking a set of corresponding high-fidelity (unfiltered) solutions, integrating these in time and subsequently filtering the solutions again. Clearly, this is computationally expensive. Instead, we will stochastically perturb the low-fidelity solution after a time step has been completed, where the perturbation is independent of the solution state. The perturbation is based on measurements of $M(u)$. Thus, a prediction ensemble provides a Monte Carlo approximation of the distribution of expected solution states. We will further specify the adopted perturbation in Section 3.2. Briefly, the prediction step is described as

$$\mathbb{P}(w_n|\tilde{u}_n) \rightarrow \mathbb{P}(w_{n+1}|\tilde{u}_n). \quad (7)$$

The resulting distribution will generally not equal the ideal distribution and may be markedly different when errors accumulate after long simulation times. We assume that the solutions in the ideal distribution are characterized by measured statistics from the filtered high-fidelity data and will use this information to nudge the stochastically perturbed solutions toward solutions that are more likely to be in the ideal distribution.

Finding probability distributions given observations of the underlying dynamical system has traditionally been the goal of data assimilation [48]. Data assimilation aims to combine model predictions with observational data in a manner that optimally balances the uncertainties present in both the predictions and the observations. Filtering approaches in data assimilation deal with determining the state of a dynamical system using data from the past up to the present. This is commonly achieved by sequentially updating the pdf of the variable of interest in the so-called filtering update. The update consists of two steps referred to as the prediction, shown in (7), followed by the analysis

$$\mathbb{P}(w_{n+1}|\tilde{u}_n) \rightarrow \mathbb{P}(w_{n+1}|\tilde{u}_{n+1}). \quad (8)$$

The distribution of LES solutions will be updated in the analysis step by incorporating knowledge of the ideal distribution, with the aim of yielding LES solutions which are more likely to be in the ideal distribution. A common way to include information into a prediction ensemble is via Bayes' theorem [61, 59]. This has led to DA schemes for nonlinear problems such as the ensemble Kalman filter (EnKF) [29, 30] and particle filters [9].

The chaotic behavior of turbulent flow motivates reproducing flow statistics rather than pointwise flow values with a computational model. Therefore, the analysis (8) will be carried out by assimilating statistics of the high-fidelity solution \tilde{u}_{n+1} into the predicted LES solution w_{n+1} . We assume that the ideal distribution is characterized by user-specified flow statistics or quantities of interest (QoIs). Furthermore, we assume that the flow is statistically stationary, and that the statistical properties of each QoI are fixed and known beforehand from available high-fidelity data. As a modeling approach, one can therefore generate 'observations' by sampling each QoI from an estimated distribution. Once the observation is available, a DA scheme is used to assimilate the observed statistics into the predicted ensemble. Subsequently, the assimilated statistics must be enforced in the numerical solution to complete the correction.

The prediction-analysis turbulence closure modeling framework presented here requires several modeling choices. The prediction step requires one to choose how to (i) measure the sub-grid force (6)

and (ii) apply the ensuing stochastic perturbations. In the analysis step, one must decide (iii) which statistics to assimilate, (iv) how the ‘observations’ are defined and (v) which DA scheme is used to nudge the solution. In the following section, we provide an example for Rayleigh-Bénard convection and highlight the adopted modeling choices.

3 Application to Rayleigh-Bénard convection

In this section, we introduce the governing equations and the test case that the closure model will be applied to. Subsequently, we elaborate on the model choices, provide implementation details and an estimate of the resulting computational complexity.

3.1 Governing equations and numerical methods

Two-dimensional Rayleigh-Bénard (RB) convection serves as the test bed for the proposed model. The equations governing RB convection are given by incompressible Navier-Stokes equations coupled to an energy equation describing buoyancy effects under the Boussinesq approximation. The nondimensionalized equations are

$$\frac{\partial \mathbf{u}}{\partial t} + \mathbf{u} \cdot \nabla \mathbf{u} = \frac{Pr}{Ra} \nabla^2 \mathbf{u} - \nabla p + T \mathbf{e}_y, \quad (9)$$

$$\nabla \cdot \mathbf{u} = 0, \quad (10)$$

$$\frac{\partial T}{\partial t} + \mathbf{u} \cdot \nabla T = \frac{1}{\sqrt{Pr Ra}} \nabla^2 T, \quad (11)$$

where \mathbf{u} is the velocity, p is the pressure, T is the temperature, and \mathbf{e}_y is the unit vector in the vertical direction. The equations are solved in a two-dimensional rectangular box of width $L_x = 2$ and height $L_y = 1$. Periodic boundary conditions are imposed on the sides of the domain for all variables. The top and bottom boundaries are walls with no-slip boundary conditions for the velocity, and prescribed values of 1 at the bottom and 0 at the top for the dimensionless temperature. The dimensionless numbers are the Prandtl number $Pr = \nu/\kappa$ and the Rayleigh number $Ra = g\beta\Delta L_y^3/(\nu\kappa)$. These numbers describe the ratio of characteristic length scales of the velocity and the temperature and the ratio between buoyancy and viscous effects, respectively, and we have a Reynolds number $Re = \sqrt{Ra/Pr}$. Here ν is the kinematic viscosity, κ is the thermal diffusivity, g is the gravitational acceleration, β is the thermal expansion coefficient, Δ is the temperature difference between the walls of the domain. The test case is run at $Pr = 1$ and $Ra = 10^{10}$ to simulate in the turbulent convective regime.

The equations (9-11) are discretized in space using a energy-conserving finite difference method [69]. The high-fidelity solver is parallelized following [15]. The velocity is defined on a staggered grid, the temperature is defined on the same grid as the vertical velocity, and the pressure is computed at the cell centers. The arrangement of the temperature and vertical velocity ensures no interpolation errors when computing the buoyancy term [68]. A hyperbolic tangent grid spacing is adopted in the vertical (wall-normal) direction, guaranteeing refinement near the walls to resolve the boundary layer. The grid is uniformly spaced in the horizontal direction.

The temporal discretization follows from a fractional-step third-order Runge-Kutta (RK3) for explicit terms and the Crank-Nicholson (CN) scheme for implicit terms. A time step from t^n to t^{n+1} is divided into three sub-stages denoted by the superscript $j, j = 0, 1, 2$, where $j = 0$ coincides with the situation at t^n . In each stage, a provisional velocity \mathbf{u}^* is computed as

$$\frac{\mathbf{u}^* - \mathbf{u}^j}{\Delta t} = \left[\gamma_j H^j + \rho_j H^{j-1} - \alpha_j \mathcal{G} p^j + \alpha_j \mathcal{A}_y^j \frac{\mathbf{u}^* + \mathbf{u}^j}{2} \right]. \quad (12)$$

The Runge-Kutta coefficients γ, ρ, α are given by $\gamma = [8/15, 5/12, 3/4], \rho = [0, -17/60, -5/12]$ and $\alpha = \gamma + \rho$ [58, 68, 15]. The discrete gradient is denoted by \mathcal{G} . The convective terms, horizontal diffusion terms and source terms (buoyancy) are collected in H^j and are treated explicitly. The vertical diffusion term \mathcal{A}_y is treated implicitly to eliminate viscous stability restrictions arising from the non-uniform grid near the boundary [46]. A Poisson equation is then solved using \mathbf{u}^* to impose

the continuity constraint (10). Discretely, this is given by

$$\mathcal{L}\phi = \frac{1}{\alpha_j \Delta t} (\mathcal{D}\mathbf{u}^*), \quad (13)$$

where \mathcal{L} is the discrete Laplacian and \mathcal{D} is the discrete divergence. The velocity and pressure are then updated to yield a divergence-free velocity field,

$$\mathbf{u}^{j+1} = \mathbf{u}^* - \alpha_j \Delta t (\mathcal{G}\phi), \quad (14)$$

$$p^{j+1} = p^j + \phi - \frac{\alpha_j \Delta t}{2Re} (\mathcal{L}\phi). \quad (15)$$

The QUICK interpolation scheme [50] is used to discretize the convective terms, whereas the diffusive terms are discretized with a standard second-order finite difference scheme in both spatial directions. Finite differences are used to define the discrete gradient \mathcal{G} , the discrete divergence \mathcal{D} and the discrete Laplacian \mathcal{L} .

A resolution of 4096×2048 is adopted for the DNS, which has been shown to be sufficient to resolve the flow at the chosen Rayleigh number [70]. All subsequent coarse-grid simulations are carried out on a 64×32 grid. The flow cannot be fully resolved at this low resolution and the numerical method induces artificial dissipation [38, 24]. Hence, the low-fidelity numerical solution will reach a different statistically state than the high-fidelity reference solution if no model is explicitly applied.

3.2 Model specification

Following Section 2, the model consists of a stochastic perturbation and a subsequent statistical correction. In the first step, one has to choose (i) how to measure the sub-grid force (6) and (ii) how to apply the stochastic perturbations based on these data. In the second step, the choices condense to (iii) which statistics to assimilate, (iv) how to generate ‘observations’ based on the statistics of the high-fidelity data and (v) which DA scheme to use for the nudging procedure. These modeling choices are highlighted below.

We employ a simple *a posteriori* method to measure the subgrid force $M(u)$ in (6). Specifically, $M(u)$ is measured by integrating the high-fidelity solver in time from solution u and the low-fidelity solver from \tilde{u} . Both solutions are integrated for a single time step, after which the solution from the high-fidelity solver is filtered and compared to the solution of the low-fidelity solver. The measurement approximates $M(u)$ since the difference between the two fields is taken after a discrete time step. More elaborate methods of *a posteriori* measurements have been used in recent studies (see [64] and references therein), but will not be considered in the current study.

The periodicity of the domain in the horizontal (wall-parallel) direction permits computing the one-dimensional Fourier transform along horizontal cross sections of the domain. We use this to define the stochastic perturbations and the QoIs which will be assimilated. The perturbations are chosen and implemented as follows. Time series of magnitudes of spectral coefficients are known from the *a posteriori measurements* in each horizontal profile, for each prognostic variable. The means and variances are used to define a normal distribution, independently for each magnitude. In the perturbation, all spectral coefficients are assigned a magnitude, sampled from its corresponding normal distribution, and a phase, drawn independently from a uniform distribution over $[0, 2\pi]$. The corresponding physical fields are added as a perturbation after the full time step has been completed, which can accurately compensate for coarsening errors even when a fraction of data is used [25] and is non-intrusive, thereby readily enabling ensemble forecasts. Temporal correlation effects and covariances between the different spectral coefficients are excluded in the perturbations. Including the latter properties is left for future work.

The quantities of interest are chosen as the energy spectra and mean heat flux in all horizontal cross-sections of the domain. Once the desired energy is known in a horizontal cross-section, the magnitudes of the Fourier coefficients in that cross-section can be adjusted exactly and the physical solution can be reconstructed. The desired heat flux values are approximated in the physical solution by applying a gradient descent method on the phases of the Fourier coefficients of the temperature, as developed in [24].

All specified statistics are assigned a random value in an ‘observation’, where each value is based on the available high-fidelity data. The current adaptation of the model uses only the measured mean

values and variances of each statistic to define separate distributions from which the random values are drawn. Here, the observed values for each statistic are sampled from normal distributions with the corresponding measured mean and variance, independently for each statistic at each time step. The number of observations generated in each analysis step equals the prediction ensemble size.

A simplified ensemble Kalman filter (EnKF) [29] is employed here to nudge the predictions toward the observations. EnKF takes into account the nonlinearity of the governing equations, permits using a wide range of noise models [30], and is straightforward to implement. A diagonalization approach [42, 52] is used, thereby disregarding covariances between the QoIs, so that the analysis acts on each QoI separately. This avoids computing (inverses of) covariance matrices in the analysis step as is usually required in EnKF, which becomes a source of extensive computational costs if many statistics are assimilated simultaneously. Instead, the analysis for each QoI reduces to a scalar equation independent of other QoIs. Denoting a QoI in a forecast ensemble member j by ψ_j^f , the analysis step in the diagonal EnKF scheme yields an updated value ψ_j^a as

$$\psi_j^a = \psi_j^f + \left(\frac{\sigma_e^f}{\sigma_e^f + \sigma_o} \right) (d_j - \psi_j^f). \quad (16)$$

Here σ_e^f is the sample variance of the QoI in the prediction ensemble, σ_o is the sample variance of the QoI in the observations, and d_j is the j^{th} observed instance of the QoI. The balance between the uncertainties in the prediction ensemble and the observations, $\sigma_e^f/(\sigma_e^f + \sigma_o)$, is referred to as the gain and determines the nudging strength toward the observation.

3.3 Computational complexity

We now provide some estimates of the complexity reduction when employing the model on coarse grids. Solving the Poisson equation (13) is the largest source of computational costs in the spatial discretization since it involves solving a sparse $(N_x N_y) \times (N_x N_y)$ linear system. The high-fidelity solver employs a parallelization technique for finite-difference discretization of wall-bounded flows [68] which solves (13) in $\mathcal{O}(N_x N_y \log[N_y])$ operations. The low-fidelity solver uses a standard LU factorization for sparse linear systems for this purpose, requiring $\mathcal{O}((N_x N_y)^{3/2})$ computational steps [35].

The one-dimensional (inverse) fast Fourier transform (IFFT) along horizontal cross-sections of the domain is used extensively in the present adaptation of the model. These are computed in $\mathcal{O}(N_x \log[N_x])$ operations [40]. The random sub-grid scale fields for the stochastic perturbations are computed by applying the IFFT at each horizontal profile for all prognostic variables. During the nudging procedure, the (I)FFT is computed twice for these variables. The heat flux correction requires three computations of the (I)FFT in total and an additional $\mathcal{O}(N_x N_y)$ arithmetic operations per iteration. In total, we obtain the estimates of $\mathcal{O}(10^7)$ operations per time step for the high-fidelity solver, and $\mathcal{O}(10^5)$ for the low-fidelity solver including the model.

The time step size becomes restrictive for high- Ra flow. A step size of $\mathcal{O}(\Delta y) \approx \mathcal{O}((Ra Nu)^{-1}) = \mathcal{O}(10^{-12})$ is suggested [68] to fully resolve the turbulent flow features. Here Δy denotes the smallest grid spacing in the non-uniform wall-normal grid. A time step size of $\mathcal{O}(10^{-2})$ was found to yield stable results on the coarse grids, likely due to the presence of artificial dissipation, leading to a significant computational cost reduction.

4 Model performance assessment

This section presents simulation results on the coarse computational grid, comparing four models to the high-fidelity reference. Two data sets are considered for calibrating the model, for which we assess short-time and long-time simulation results computed outside of the calibration data sets. We introduce the tested models, used data sets, and assessment metrics before proceeding to the results.

Four different coarse-grid configurations are compared to the reference filtered DNS. The no-model coarse numerical simulation serves as a physics-inspired closure model. A Smagorinsky eddy viscosity model [66, 55] was additionally implemented and tested for several Smagorinsky constants, all of which yielded results similar to the no-model case due to the artificial dissipation native to the coarse discretization. These results are not shown here and instead we focus on the no-model coarse simulation. Three ensemble methods are compared. The first uses only the stochastic perturbations as described

in Section 3.2. The second ensemble uses a heuristic nudging approach towards observed statistics [24], where a nudge is defined for each statistic independently with a nudging strength defined by the measured correlation time of the corresponding statistic. The third ensemble employs the stochastic perturbation and statistical correction as presented in Section 3.2. The ensemble methods are referred to in the coming figures as ‘random sgs’, ‘statistical nudge’ and ‘random sgs, assimilated’, respectively. The ensembles will generally consist of 10 members, an ensemble with 50 members will also be discussed to investigate the prediction quality dependence on the ensemble size.

Two reference data sets are used, both extracted from a sequence of snapshots from a filtered DNS performed on a 4096×2048 computational grid. The first data set is comprised of 1000 solution snapshots each separated by 0.05 time units, in total spanning 50 time units. The second set consists of 20 solution snapshots each separated by 0.5 time units, spanning 10 time units. The first snapshot in both sets is taken at the same time instance which we will denote by t_0 . The choice of data sets helps verify the robustness of the model in the sparse data regime, and they will be referred to as ‘plenty data’ and ‘few data’, respectively. The *a posteriori* measurements are taken by initializing the flow from the snapshots in the data set and comparing the low-fidelity prediction to the reference after 0.05 time units. A time series for each streamwise wavenumber and heat flux at each y -coordinate is computed by measuring the quantities of interest at each snapshot. The means and variances of these time series are used in the model. The initial condition for the subsequent simulations are filtered DNS snapshots outside of the data sets. For the long-time comparison, we select the initial condition as the snapshot at $t_0 + 100$, for the short-time comparison we adopt $t_0 + 150$, $t_0 + 200$ and $t_0 + 250$.

Several metrics are used to assess the model performance. A global comparison of a solution (\mathbf{u}, T) to the reference for short lead times is provided by the pattern correlation

$$\frac{\langle (\mathbf{u}, T), (\mathbf{u}_{\text{ref}}, T_{\text{ref}}) \rangle}{\sqrt{\langle (\mathbf{u}, T), (\mathbf{u}, T) \rangle \langle (\mathbf{u}_{\text{ref}}, T_{\text{ref}}), (\mathbf{u}_{\text{ref}}, T_{\text{ref}}) \rangle}}, \quad (17)$$

where $\langle \cdot, \cdot \rangle$ denotes the standard L^2 inner product over the computational domain. Long-time simulation results are evaluated via time-averaged energy spectra and root-mean-square deviations (r.m.s.) and rolling means of the kinetic energy (KE) and the Nusselt number. The r.m.s. is computed as a function of the wall-normal distance. For a given y -value, we compute the r.m.s. of a field f as

$$\text{r.m.s.}(f, y, t) = \left[\frac{1}{|A|} \int_A (f(x, y, t) - \langle f(x, y, t) \rangle_A)^2 \text{d}A \right]^{1/2}, \quad (18)$$

where $\langle \cdot \rangle_A$ is the mean over a cross-section with length $|A|$. The KE and the Nusselt number are defined as

$$\text{KE} = \int_{\Omega} \frac{1}{2} (\mathbf{u} \cdot \mathbf{u}) \text{d}\Omega, \quad (19)$$

$$\text{Nu} = 1 + \sqrt{\text{Pr} \text{Ra} \langle vT \rangle_{\Omega}}, \quad (20)$$

where $\langle \cdot \rangle_{\Omega}$ is the mean over the entire domain Ω . The Nusselt number describes the heat flux from the bottom to the top of the domain and is one of the critical responses of the system to the imposed physical parameters [3]. The definition (20) is particularly suited for computation on coarse grids since it does not involve any gradients.

4.1 Model performance with plenty data

We first assess the model performance when plenty data is used to estimate the model parameters.

The pattern correlations (17) at short lead times are shown in figure 1 for three distinct initial conditions. The no-model simulation deteriorates over time due to loss of details in the numerical solution after initializing the flow from a filtered DNS snapshot. A low correlation does not imply that the flow statistics are incorrect since it measures the likeness of the global solution to the reference. Rather, it indicates the rate at which the flow deviates from the reference. It allows us to distinguish whether a solution is too rapidly steered towards a configuration with the desired statistical flow features. The correlation of the statistical nudging ensemble with the reference decreases rapidly, from which we surmise that the ad-hoc nudging is too strong and does not lead to a physical flow evolution. Applying the stochastic perturbation largely mitigates this. The difference between the ensemble with

random perturbations and the ensemble with perturbations and assimilated statistics suggests that a reduced nudging strength might be favorable when the initial condition is known. For example, this can be achieved by incorporating temporal effects into the observations, thereby including information of the initial conditions in the observation. Alternatively, a dynamically adaptive nudging procedure [4] can be applied such that a nudge is only applied if it increases the likelihood of the solution being in the ideal distribution.

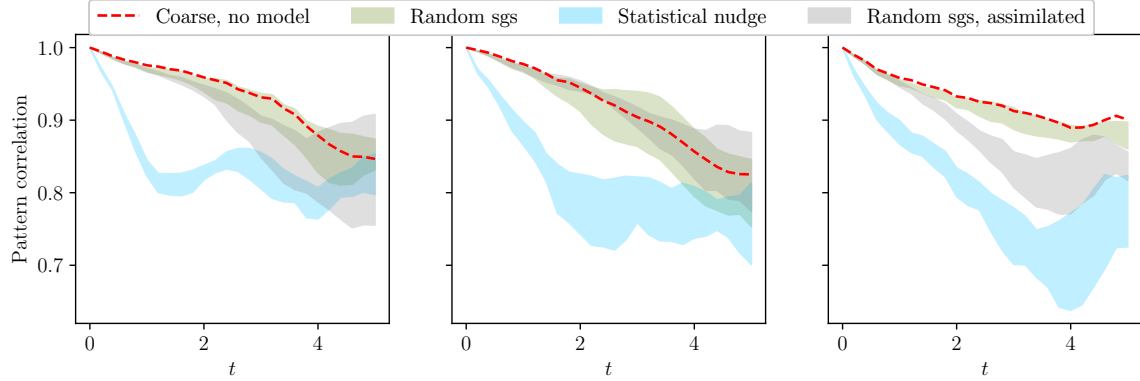


Figure 1: Pattern correlation between the prediction and the reference solution, using plenty data to calibrate the model. Three different initial conditions are considered. Each ensemble consists of 10 members; each band is colored between the maximal and minimal measured values.

A qualitative model comparison is given in figure 2 through instantaneous flow snapshots after reaching a statistically steady state in a long-time simulation. We observe that the no-model simulation suffers from artificial dissipation, evident from the smoothed fields and the reduced velocity magnitudes. The level of detail in the velocity fields is reconstructed well with the ensemble methods. The temperature fields display small-scale details, but these are fragmented instead of forming coherent patterns. Simultaneously, the velocity fields of the nudged ensembles feature pronounced flow details and maintain a qualitative agreement with the reference.

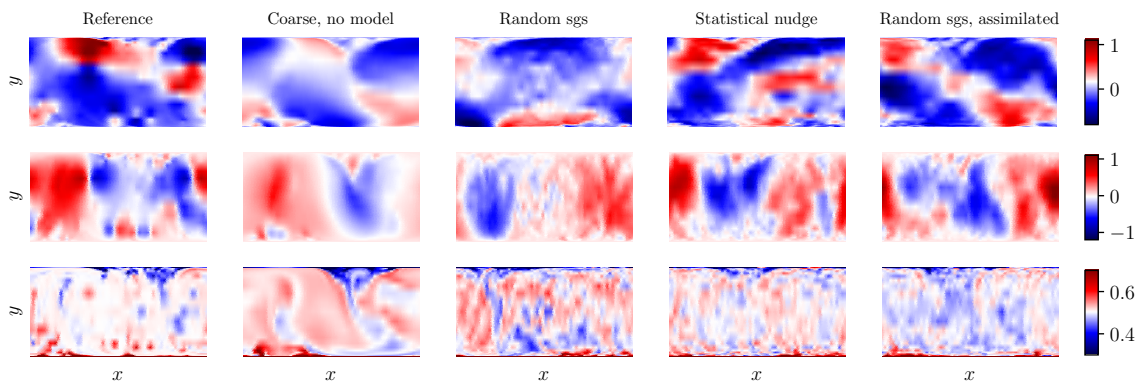


Figure 2: Instantaneous snapshots after simulating for 100 time units initialized from a filtered DNS snapshot. Shown are the horizontal velocity (top row), vertical velocity (middle row) and temperature (bottom row). A snapshot from a single ensemble member is shown for the ensemble methods.

The average energy spectra near the center of the domain are depicted in figure 3, where the average is taken over all snapshots and all ensemble members. We also display the average spectra of the high-fidelity measurements that comprise the data set from which the model parameters are extracted and refer to this as the training data. The no-model simulation provides predictions that consistently contain too little energy. Only applying the stochastic perturbation does not adequately alleviate this. Applying a correction, either ad-hoc or by assimilating statistics, yields a significant improvement particularly at the largest resolvable scales. This suggests that incorporating high-fidelity

data into the model benefits the prediction of flow statistics in long-time simulations. We observe that the resulting energy spectra approximate the training data accurately, which itself slightly deviates from the reference spectra over the simulated interval.

The time-averaged r.m.s. values of show considerable improvement when applying the correction procedure, as shown in figure 4. Only applying the stochastic perturbation yields no improvement over using no model in the long-time simulations, which further highlights the added value of the statistical correction. Assimilating statistics leads to a pronounced improved of the velocity r.m.s. particularly near the center of the domain. Here, the grid size is largest and the discretization effects significant, which induce a large measured sub-grid force and thus large stochastic perturbations. In turn, these large perturbations lead to a larger gain factor in the correction (16) and a close adherence to the reference statistics.

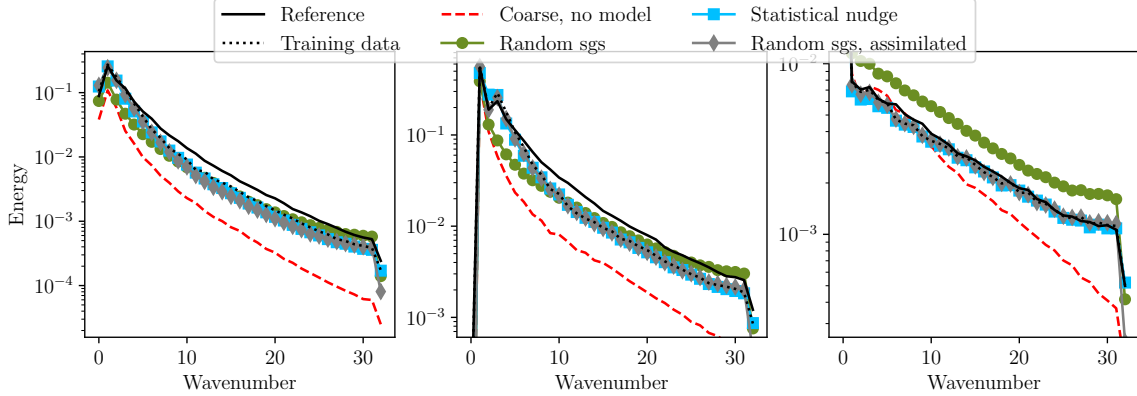


Figure 3: Time-averaged energy spectra measured along a horizontal cross-section of the domain for the horizontal velocity (left), vertical velocity (middle) and temperature (right). The cross-sections are taken in the core of the domain at $y = 5.5 \times 10^{-1}$ for the horizontal velocity and $y = 5.0 \times 10^{-1}$ for the vertical velocity and the temperature.

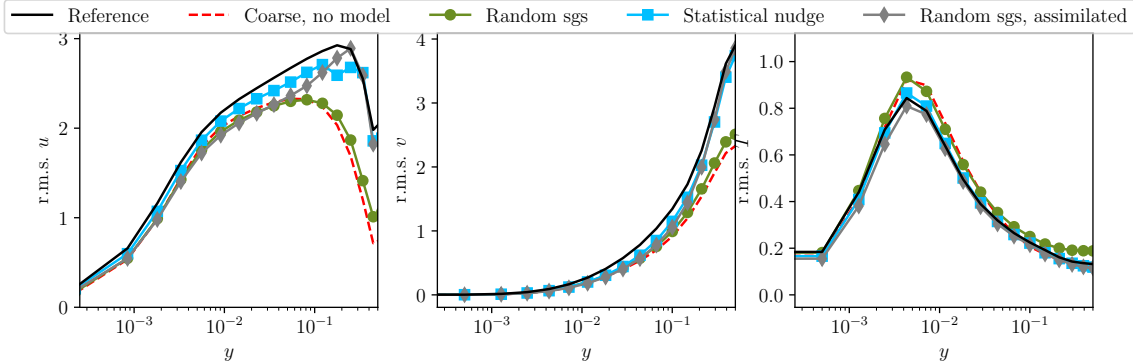


Figure 4: Average root mean square (r.m.s.) of the horizontal velocity (left), vertical velocity (middle) and temperature (right), measured along horizontal cross-sections of the domain and shown as functions of the wall-normal distance.

The rolling averages of the total kinetic energy and the Nusselt number over time are respectively given in figures 5 and 6. The artificial dissipation in the coarsened discretization causes the no-model result to deviate from the filtered DNS and reach a different statistically steady state with a strongly reduced energy content. Only applying the stochastic perturbation does not alleviate this, whereas including high-fidelity statistical data substantially improves the total energy content. An improvement of the predicted Nusselt number is observed for all ensemble methods. Notably, this includes the ensemble in which the predictions are perturbed and no knowledge of the heat flux

is included. However, judging from the energy spectra in figure 3, this result is obtained without correctly predicting the energy distributions in the velocity and temperature fields.

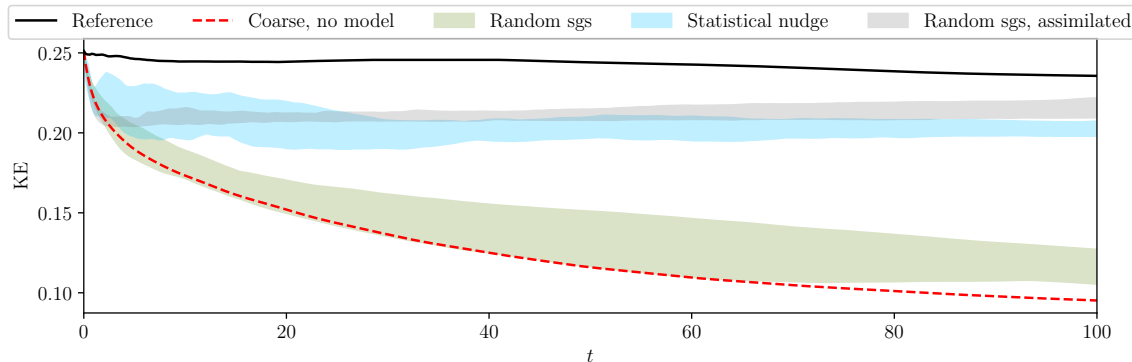


Figure 5: Rolling mean of the kinetic energy (KE) number over time.

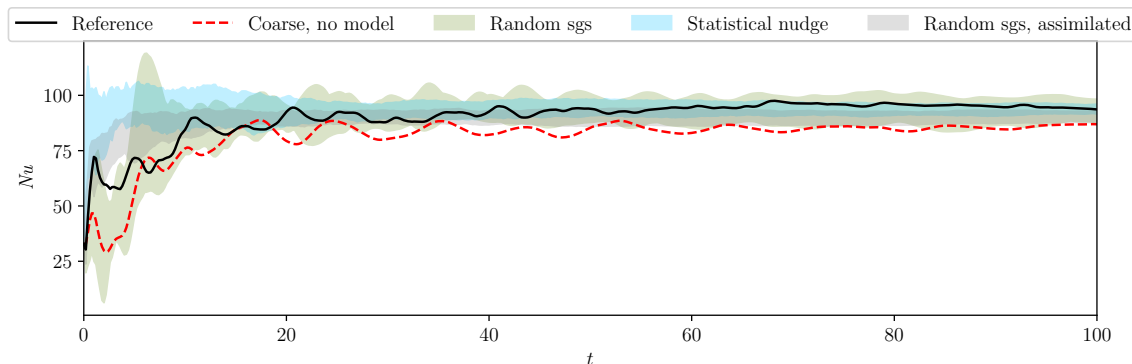


Figure 6: Rolling mean of the Nusselt number (Nu) over time.

4.2 Model performance with few data

We now turn our attention to the model performance when using few data to estimate the model parameters. Only 20 snapshots are used to measure the the sub-grid scale forcing and the reference statistics. As such, the means and variances used in the model are poorly estimated and the correlation times of the quantities of interest become difficult to estimate due the sparsity of the data. We therefore expect the quality of the ad-hoc statistical nudging method to decrease.

The pattern correlations for short lead times are given in figure 7. No significant change in prediction quality is observed, compared to the predictions based on plenty data in figure 1. This suggests that the prediction of the instantaneous solution at short lead times is robust under changes in the available data and instead relies on the accuracy of the initial condition.

The energy spectra in the core of the domain and the average r.m.s. values for the prognostic variables are depicted in figures 8 and 9, respectively. Good agreement is observed at the largest scales of motion despite the small amount of data, and the methods that employ a statistical correction adequately reproduce the energy in these scales. The effects of using limited data become apparent in the smaller scales of motion, particularly visible in the spectrum of the temperature. The average measured energy in these scales is not converged and hence deviate from the reference. The ensemble with assimilated statistics closely follows the training data, for which an improvement over the no-model result is still evident. The average r.m.s. values do not deteriorate using the small data set and show good agreement with the reference. The rolling averages of the kinetic energy and the Nusselt number, respectively shown in figures 10 and 11, display the same qualitative behavior is observed

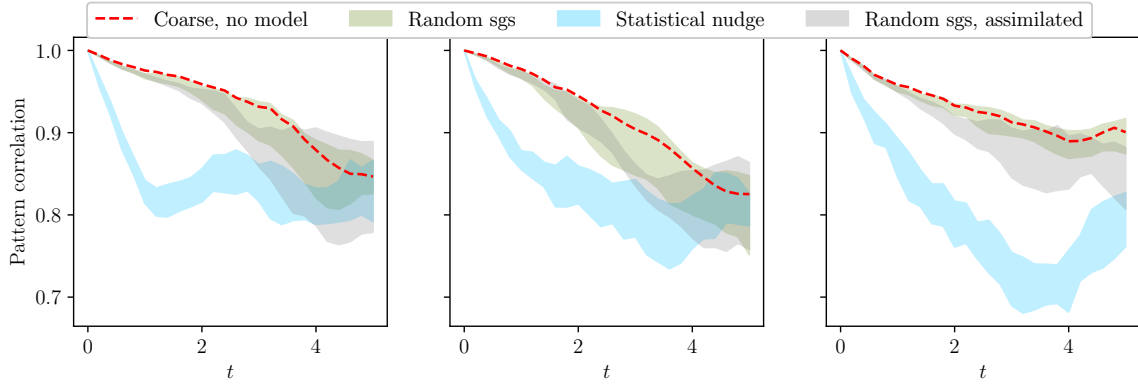


Figure 7: Pattern correlation between the prediction and the reference solution, using few data to calibrate the model. Three different initial conditions are considered. Each ensemble consists of 10 members; each band is colored between the maximal and minimal measured values.

as when using plenty data. Overall, no distinct loss of predictive quality is found using few data to calibrate the model when compared to using plenty data.

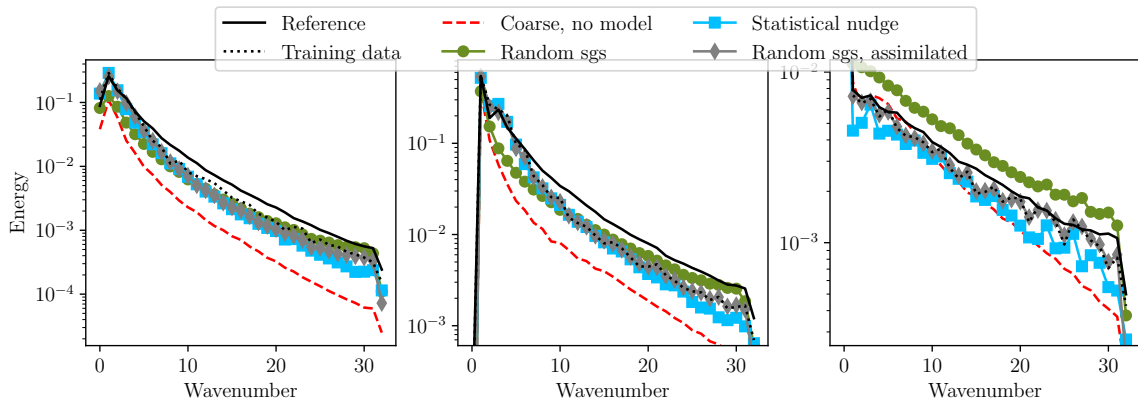


Figure 8: Time-averaged energy spectra measured along a horizontal cross-section of the domain for the horizontal velocity (left), vertical velocity (middle) and temperature (right). The cross-sections are taken in the core of the domain at $y = 5.5 \times 10^{-1}$ for the horizontal velocity and $y = 5.0 \times 10^{-1}$ for the vertical velocity and the temperature.

4.3 Dependence on ensemble size

The EnKF results in the optimal linear estimator in the limit of large ensemble size [49, 65]. Carrying out an ensemble simulation with many ensemble members might quickly become prohibitively expensive, even when using a computationally cheap low-fidelity solver. In the EnKF, the evolution of the individual ensemble members is coupled through the analysis step which uses information of the entire ensemble, and a change in system dynamics may thus be observed when changing the number of ensemble members. We therefore repeat the short-time numerical simulations presented in figure 1 in Section 4.1 using 50 ensemble members instead of 10 to establish that a modest ensemble size does not adversely affect the model performance. The obtained pattern correlations in figure 12 show no qualitative change with respect to the earlier presented results. This suggests that the currently adopted approach already provides robust forecasts at small ensemble size.

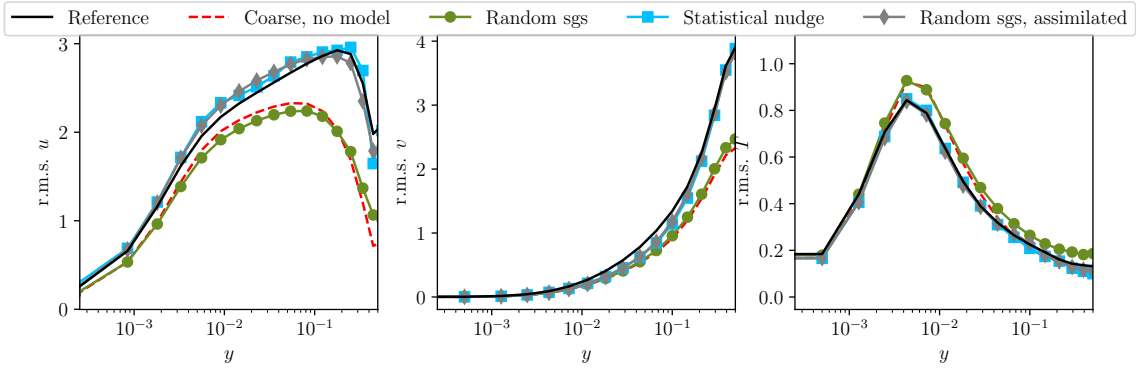


Figure 9: Average root mean square (r.m.s.) of the horizontal velocity (left), vertical velocity (middle) and temperature (right), measured along horizontal cross-sections of the domain and shown as functions of the wall-normal distance.

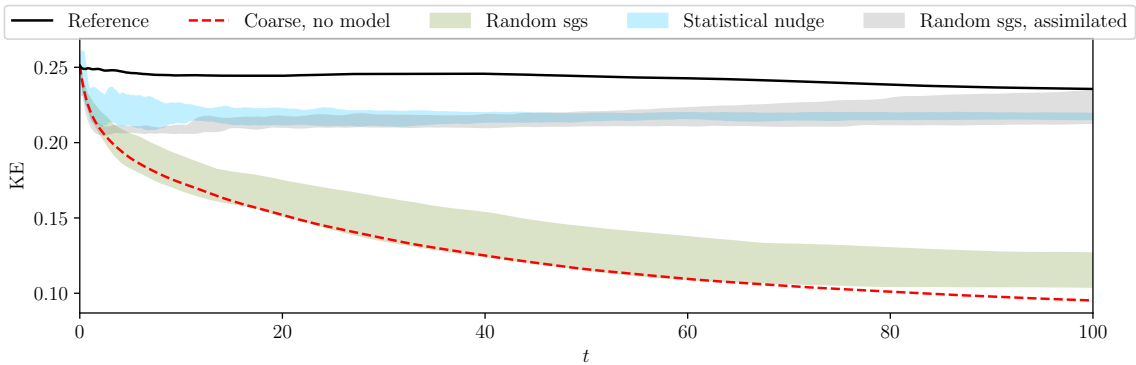


Figure 10: Rolling mean of the kinetic energy (KE) number over time.

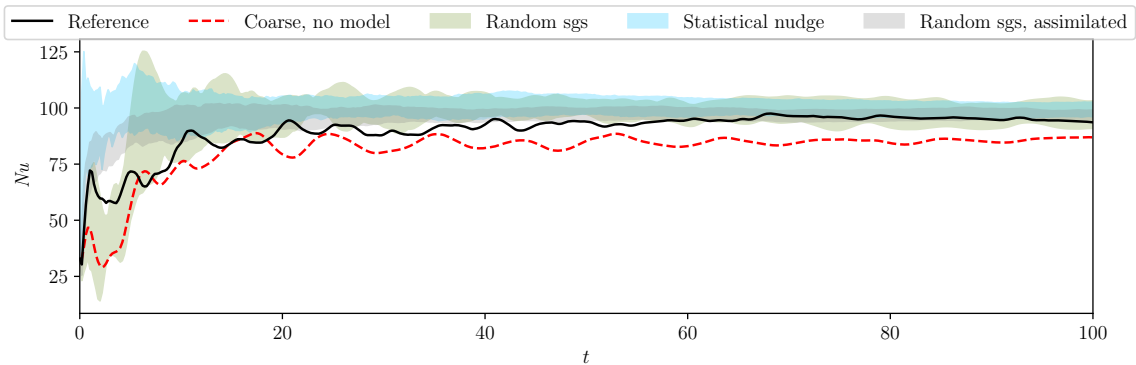


Figure 11: Rolling mean of the Nusselt number (Nu) over time.

5 Conclusions

In this paper, we have proposed a method for deriving probabilistic data-driven turbulence closure models suitable for coarsened steady-state turbulence. Based on *ideal large-eddy simulation*, a combination of stochastic forcing and data assimilation methods is suggested, requiring both *a posteriori* collected data of the employed numerical solver and statistical data of the high-fidelity solution. Thus, the method exploits knowledge of the local integration error and the desired flow statistics.

The model was demonstrated using a non-intrusive implementation applied to two-dimensional Rayleigh-Bénard convection at Rayleigh number $Ra = 10^{10}$. Stochastic perturbations based on sub-

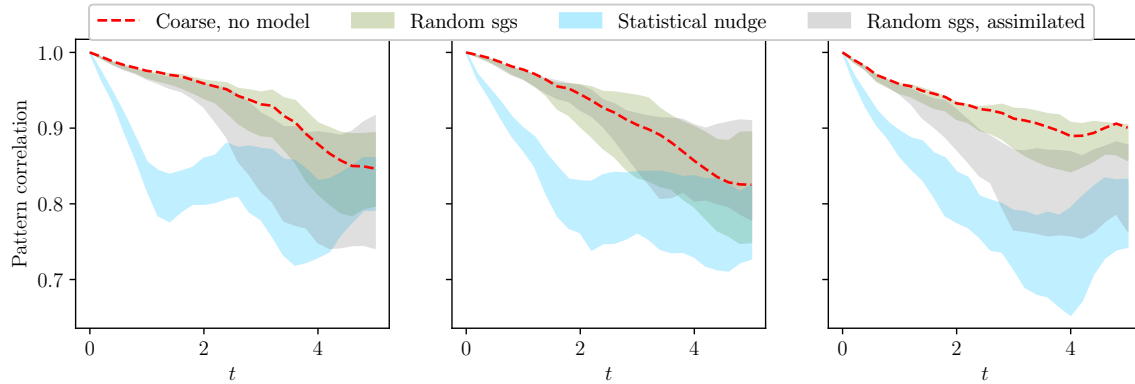


Figure 12: Pattern correlation between the prediction and the reference solution, using plenty data to calibrate the model. Each ensemble consists of 50 members; each band is colored between the maximal and minimal measured values.

grid scale data were used in conjunction with a simplified ensemble Kalman filter to steer coarse numerical predictions towards desired statistics known from a precursor simulation. Here, we focused on horizontal energy spectra and average heat flux, which were found to be accurately reproduced with the proposed model. The model showed robust results for a modest ensemble size. No considerable deterioration of the predictions was observed using as few as 20 high-fidelity snapshots to determine the model parameters.

The presented modeling framework is general and can be applied to different fluid dynamical models. Nonetheless, many modeling choices have to be made in the actual implementation. Exploring different modeling choices is a challenge for future work. Notably, the current adopted implementation disregarded all covariances between the chosen quantities of interest. A promising approach to include these covariances without substantially increasing the computational cost associated to the model, is to significantly reduce the number of quantities of interest [44]. Adopting a smaller number of key statistics additionally makes it more tractable to compare different data assimilation schemes within the modeling framework.

Software and data availability The data and adopted implementations that support the findings of this study are publicly available in Zenodo at <http://doi.org/10.5281/zenodo.13353273>.

Declaration of interests. The authors report no conflict of interest.

References

- [1] Ronald J Adrian. “On the role of conditional averages in turbulence theory”. In: (1975).
- [2] Syver Døving Agdestein and Benjamin Sanderse. “Discretize first, filter next: learning divergence-consistent closure models for large-eddy simulation”. In: *arXiv preprint arXiv:2403.18088* (2024).
- [3] Guenter Ahlers, Siegfried Grossmann, and Detlef Lohse. “Heat transfer and large scale dynamics in turbulent Rayleigh-Bénard convection”. In: *Reviews of modern physics* 81.2 (2009), pp. 503–537.
- [4] Ömer Deniz Akyildiz and Joaquín Míguez. “Nudging the particle filter”. In: *Statistics and Computing* 30 (2020), pp. 305–330.
- [5] MU Altaf et al. “Downscaling the 2D Bénard convection equations using continuous data assimilation”. In: *Computational Geosciences* 21 (2017), pp. 393–410.
- [6] HM Arnold, IM Moroz, and TN Palmer. “Stochastic parametrizations and model uncertainty in the Lorenz’96 system”. In: *Philosophical Transactions of the Royal Society A: Mathematical, Physical and Engineering Sciences* 371.1991 (2013), p. 20110479.

- [7] Abderrahim Azouani, Eric Olson, and Edriss S Titi. “Continuous data assimilation using general interpolant observables”. In: *Journal of Nonlinear Science* 24 (2014), pp. 277–304.
- [8] Eviatar Bach et al. “Filtering dynamical systems using observations of statistics”. In: *Chaos: An Interdisciplinary Journal of Nonlinear Science* 34.3 (2024).
- [9] Alan Bain and Dan Crisan. *Fundamentals of stochastic filtering*. Vol. 3. Springer.
- [10] Andrea Beck, David Flad, and Claus-Dieter Munz. “Deep neural networks for data-driven LES closure models”. In: *Journal of Computational Physics* 398 (2019), p. 108910.
- [11] Gal Berkooz, Philip Holmes, and John L Lumley. “The proper orthogonal decomposition in the analysis of turbulent flows”. In: *Annual review of fluid mechanics* 25.1 (1993), pp. 539–575.
- [12] Dirk Blömker et al. “Accuracy and stability of the continuous-time 3DVAR filter for the Navier–Stokes equation”. In: *Nonlinearity* 26.8 (2013), p. 2193.
- [13] Roberto Buizza, M Milleer, and Tim N Palmer. “Stochastic representation of model uncertainties in the ECMWF ensemble prediction system”. In: *Quarterly Journal of the Royal Meteorological Society* 125.560 (1999), pp. 2887–2908.
- [14] Elizabeth Carlson, Adam Larios, and Edriss S Titi. “Super-Exponential Convergence Rate of a Nonlinear Continuous Data Assimilation Algorithm: The 2D Navier–Stokes Equation Paradigm”. In: *Journal of Nonlinear Science* 34.2 (2024), p. 37.
- [15] P Cifani, JGM Kuerten, and BJ Geurts. “Highly scalable DNS solver for turbulent bubble-laden channel flow”. In: *Computers & Fluids* 172 (2018), pp. 67–83.
- [16] Colin Cotter et al. “A particle filter for stochastic advection by Lie transport: a case study for the damped and forced incompressible two-dimensional Euler equation”. In: *SIAM/ASA Journal on Uncertainty Quantification* 8.4 (2020), pp. 1446–1492.
- [17] Colin Cotter et al. “Numerically modeling stochastic Lie transport in fluid dynamics”. In: *Multiscale Modeling & Simulation* 17.1 (2019), pp. 192–232.
- [18] Philippe Courtier et al. “The ECMWF implementation of three-dimensional variational assimilation (3D-Var). I: Formulation”. In: *Quarterly Journal of the Royal Meteorological Society* 124.550 (1998), pp. 1783–1807.
- [19] Daan Crommelin and Eric Vanden-Eijnden. “Subgrid-scale parameterization with conditional Markov chains”. In: *Journal of the Atmospheric Sciences* 65.8 (2008), pp. 2661–2675.
- [20] Karthik Duraisamy. “Perspectives on machine learning-augmented Reynolds-averaged and large eddy simulation models of turbulence”. In: *Physical Review Fluids* 6.5 (2021), p. 050504.
- [21] Wouter Edeling and Daan Crommelin. “Reducing data-driven dynamical subgrid scale models by physical constraints”. In: *Computers & Fluids* 201 (2020), p. 104470.
- [22] Fourth Edition, Athanasios Papoulis, and S Unnikrishna Pillai. *Probability, random variables, and stochastic processes*. McGraw-Hill Europe: New York, NY, USA, 2002.
- [23] Sagy Ephrati et al. “Data-assimilation closure for large-eddy simulation of quasi-geostrophic flow on the sphere”. In: *arXiv preprint arXiv:2312.12858* (2023).
- [24] Sagy R Ephrati, Paolo Cifani, and Bernard J Geurts. “Data-driven spectral turbulence modelling for Rayleigh–Bénard convection”. In: *Journal of Fluid Mechanics* 975 (2023), A35.
- [25] Sagy R Ephrati et al. “Computational modeling for high-fidelity coarsening of shallow water equations based on subgrid data”. In: *Multiscale Modeling & Simulation* 20.4 (2022), pp. 1468–1489.
- [26] Sagy R Ephrati et al. “Data-Driven Stochastic Lie Transport Modeling of the 2D Euler Equations”. In: *Journal of Advances in Modeling Earth Systems* 15.1 (2023), e2022MS003268.
- [27] Sagy R Ephrati et al. “Data-driven stochastic spectral modeling for coarsening of the two-dimensional Euler equations on the sphere”. In: *Physics of Fluids* 35.9 (2023).
- [28] SR Ephrati, P Cifani, and BJ Geurts. “Stochastic data-driven pod-based modeling for high-fidelity coarsening of two-dimensional Rayleigh–Bénard turbulence”. In: *ERCOTAC Workshop Direct and Large Eddy Simulation*. Springer. 2023, pp. 209–214.

- [29] Geir Evensen. “Sequential data assimilation with a nonlinear quasi-geostrophic model using Monte Carlo methods to forecast error statistics”. In: *Journal of Geophysical Research: Oceans* 99.C5 (1994), pp. 10143–10162.
- [30] Geir Evensen. “The ensemble Kalman filter: Theoretical formulation and practical implementation”. In: *Ocean dynamics* 53 (2003), pp. 343–367.
- [31] Jorgen S Frederiksen and Steven M Kepert. “Dynamical subgrid-scale parameterizations from direct numerical simulations”. In: *Journal of the atmospheric sciences* 63.11 (2006), pp. 3006–3019.
- [32] Jorgen S Frederiksen, Vassili Kitsios, and Terence J O’Kane. “Statistical Dynamics and Subgrid Modelling of Turbulence: From Isotropic to Inhomogeneous”. In: *arXiv preprint arXiv:2407.10085* (2024).
- [33] Jorgen S Frederiksen et al. “Stochastic subgrid modelling for geophysical and three-dimensional turbulence”. In: *Nonlinear and stochastic climate dynamics*. Cambridge University Press, 2017, pp. 241–275.
- [34] Hugo Frezat et al. “A posteriori learning for quasi-geostrophic turbulence parametrization”. In: *Journal of Advances in Modeling Earth Systems* 14.11 (2022), e2022MS003124.
- [35] Alan George and Esmond Ng. “On the complexity of sparse QR and LU factorization of finite-element matrices”. In: *SIAM journal on scientific and statistical computing* 9.5 (1988), pp. 849–861.
- [36] Masakazu Gesho, Eric Olson, and Edriss S Titi. “A computational study of a data assimilation algorithm for the two-dimensional Navier–Stokes equations”. In: *Communications in Computational Physics* 19.4 (2016), pp. 1094–1110.
- [37] Bernard J Geurts. *Direct and Large-Eddy Simulation*. Vol. 1. Walter de Gruyter GmbH & Co KG, 2022.
- [38] Bernard J Geurts and Fedderik van der Bos. “Numerically induced high-pass dynamics in large-eddy simulation”. In: *Physics of fluids* 17.12 (2005).
- [39] Bernard J Geurts and Darryl D Holm. “Alpha-modeling strategy for LES of turbulent mixing”. In: *Turbulent flow computation* (2002), pp. 237–278.
- [40] Gene H Golub and Charles F Van Loan. *Matrix computations*. JHU press, 2013.
- [41] Mohamad Abed El Rahman Hammoud et al. “Continuous and discrete data assimilation with noisy observations for the Rayleigh–Bénard convection: a computational study”. In: *Computational Geosciences* 27.1 (2023), pp. 63–79.
- [42] J Harlim and AJ Majda. “Filtering nonlinear dynamical systems with linear stochastic models”. In: *Nonlinearity* 21.6 (2008), p. 1281.
- [43] Klaus Hasselmann. “Stochastic climate models part I. Theory”. In: *tellus* 28.6 (1976), pp. 473–485.
- [44] Rik Hoekstra, Daan Crommelin, and Wouter Edeling. “Reduced Data-Driven Turbulence Closure for Capturing Long-Term Statistics”. In: *arXiv preprint arXiv:2407.14132* (2024).
- [45] Darryl D Holm. “Variational principles for stochastic fluid dynamics”. In: *Proceedings of the Royal Society A: Mathematical, Physical and Engineering Sciences* 471.2176 (2015), p. 20140963.
- [46] John Kim and Parviz Moin. “Application of a fractional-step method to incompressible Navier–Stokes equations”. In: *Journal of computational physics* 59.2 (1985), pp. 308–323.
- [47] Jacob A Langford and Robert D Moser. “Optimal LES formulations for isotropic turbulence”. In: *Journal of fluid mechanics* 398 (1999), pp. 321–346.
- [48] Kody Law, Andrew Stuart, and Kostas Zygalakis. “Data assimilation”. In: *Cham, Switzerland: Springer* 214 (2015), p. 52.
- [49] Kody JH Law, Hamidou Tembine, and Raul Tempone. “Deterministic mean-field ensemble Kalman filtering”. In: *SIAM Journal on Scientific Computing* 38.3 (2016), A1251–A1279.
- [50] Brian P Leonard. “A stable and accurate convective modelling procedure based on quadratic upstream interpolation”. In: *Computer methods in applied mechanics and engineering* 19.1 (1979), pp. 59–98.

- [51] Edward N Lorenz. “Predictability: A problem partly solved”. In: *Proc. Seminar on predictability*. Vol. 1. 1. Reading, 1996.
- [52] Andrew J Majda and John Harlim. *Filtering complex turbulent systems*. Cambridge University Press, 2012.
- [53] Etienne Mémin. “Fluid flow dynamics under location uncertainty”. In: *Geophysical & Astrophysical Fluid Dynamics* 108.2 (2014), pp. 119–146.
- [54] TN Palmer. “Stochastic weather and climate models”. In: *Nature Reviews Physics* 1.7 (2019), pp. 463–471.
- [55] Shia-Hui Peng and Lars Davidson. “Comparison of subgrid-scale models in LES for turbulent convection flow with heat transfer”. In: *Turbulent Heat Transfer 2* (1998), pp. 5–24.
- [56] Ugo Piomelli, Amirreza Rouhi, and Bernard J Geurts. “A grid-independent length scale for large-eddy simulations”. In: *Journal of fluid mechanics* 766 (2015), pp. 499–527.
- [57] Stephen B Pope. “Turbulent flows”. In: *Measurement Science and Technology* 12.11 (2001), pp. 2020–2021.
- [58] Man Mohan Rai and Parviz Moin. “Direct simulations of turbulent flow using finite-difference schemes”. In: *Journal of computational physics* 96.1 (1991), pp. 15–53.
- [59] Sebastian Reich and Colin Cotter. *Probabilistic forecasting and Bayesian data assimilation*. Cambridge University Press, 2015.
- [60] Valentin Resseguier, Wei Pan, and Baylor Fox-Kemper. “Data-driven versus self-similar parameterizations for stochastic advection by lie transport and location uncertainty”. In: *Nonlinear Processes in Geophysics* 27.2 (2020), pp. 209–234.
- [61] Bojana V Rosić et al. “Parameter identification in a probabilistic setting”. In: *Engineering Structures* 50 (2013), pp. 179–196.
- [62] Amirreza Rouhi, Ugo Piomelli, and Bernardus J Geurts. “Dynamic subfilter-scale stress model for large-eddy simulations”. In: *Physical review fluids* 1.4 (2016), p. 044401.
- [63] Pierre Sagaut. *Large eddy simulation for incompressible flows: an introduction*. Springer Science & Business Media, 2005.
- [64] Benjamin Sanderse et al. “Scientific machine learning for closure models in multiscale problems: A review”. In: *arXiv preprint arXiv:2403.02913* (2024).
- [65] Claudia Schillings and Andrew M Stuart. “Analysis of the ensemble Kalman filter for inverse problems”. In: *SIAM Journal on Numerical Analysis* 55.3 (2017), pp. 1264–1290.
- [66] Joseph Smagorinsky. “General circulation experiments with the primitive equations: I. The basic experiment”. In: *Monthly weather review* 91.3 (1963), pp. 99–164.
- [67] William Snyder et al. “Reduced order model closures: A brief tutorial”. In: *Recent Advances in Mechanics and Fluid-Structure Interaction with Applications: The Bong Jae Chung Memorial Volume*. Springer, 2022, pp. 167–193.
- [68] Erwin P Van Der Poel et al. “A pencil distributed finite difference code for strongly turbulent wall-bounded flows”. In: *Computers & Fluids* 116 (2015), pp. 10–16.
- [69] AW Vreman. “The projection method for the incompressible Navier–Stokes equations: the pressure near a no-slip wall”. In: *Journal of Computational Physics* 263 (2014), pp. 353–374.
- [70] Xiaojue Zhu et al. “Transition to the ultimate regime in two-dimensional Rayleigh–Bénard convection”. In: *Physical review letters* 120.14 (2018), p. 144502.